CIC@20: Multispectral Imaging

Shoji Tominaga, Graduate School of Advanced Integration Science, Chiba University, Chiba, Japan

Abstract

A variety of multi-spectral imaging methods are discussed for acquiring spectral information from a scene. We first review conventional multispectral imaging approach. The conventional imaging systems are mostly constructed by multi-band imaging devices with different filtration mechanism at the sensor side under passive illumination. We show some imaging devices, estimation algorithms, and applications. Recently, active spectral imaging attracts much attention as promising technology. The active spectral imaging method has the possibility of recovering spectral reflectance information and estimating tristimulus values of object surface in high speed. We introduce a spectral imaging technology by synchronizing a programmable light source and a high-speed monochrome camera. Two effective applications to spectral reflectance recovery and tristimulus imager are described.

Introduction

Multispectral imaging technology is a useful technology that is now widespread in all fields related with visual information. So far a variety of multispectral imaging systems and methods have been proposed for acquiring spectral information from a scene. Figure 1 shows the number of papers related with multispectral imaging, presented in the CICs of the past 19 years as a function of CIC number. The first paper in CIC was entitled "Analysis multispectral image capture" by Peter D. Burns and Roy S. Berns, 1996 [1]. In the same year, "Multichannel vision system for estimating surface and illuminant functions" by the author was published in JOSA, 1996 [2]. Therefore we can consider that the year of 1996 was the starting point of multispectral imaging. The largest number of papers at 14 were presented in CIC19 of the last year, when MCS (Multispectral Color Science) joined to CIC.

The session titles related with multispectral imaging in the past CICs are listed as follows:

CIC6 : Input
CIC7 : Image Capture
CIC9 : Spectral Image Analysis
CIC12 : Multi-spectral / Multi-primary Systems
CIC13 : Spectral Imaging
CIC14 : Multi-spectral imaging
CIC15 : Spectral Color
CIC17 : Spectral Color
CIC19 : Multispectral Color Science (joint with 13th MCS).

The research contents cover a broad range of areas, including spectral image capture, spectral reflectance estimation, illuminant estimation, spectral image compression, color reproduction system for spectral image, and computer graphics based on spectral images. The application fields of multispectral imaging look medicine, human skin, art (mainly art paintings), and wide gamut technology in the past. However, it is quite certain that application in the field is expanding.

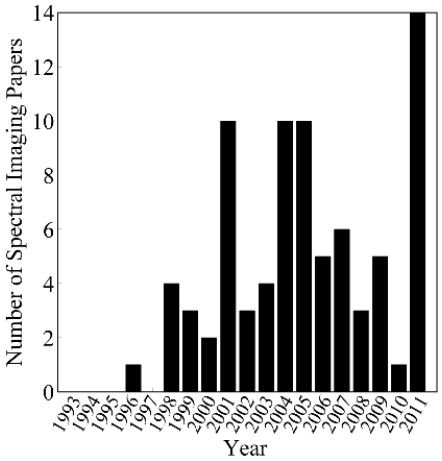

***Figure 1**. Number of papers related with multispectral imaging, presented in past 19 years.*

Some situations requiring the spectral imaging technology are as follows:

(1) An imaging system based on trichromacy faces the limitation that a color camera with three channels RGB cannot always satisfy the color matching property of the human visual system, called the Luther condition. Therefore the color camera cannot be a colorimeter.

(2) Surface-spectral reflectance exhibits a physical characteristic inherent to an object surface. Recovering the spectral reflectance functions from image sensor outputs is necessary not only for solving vision problems such as color constancy, but also for material identification and color image production. In such cases, three-channel camera has serious difficulty in estimating the accurate spectral reflectances.

(3) Spectral analysis is often needed for the detail analysis of object surfaces in a natural scene. Spectral synthesis is also needed for realistic color image production of the object surfaces under arbitrary observation conditions.

In the following, first, we will review conventional multispectral imaging approach. The conventional imaging systems are mostly constructed by multi-band imaging devices with different filtration mechanism at the sensor side under passive illumination. We will show some typical imaging devices, algorithms for estimating spectral functions, and applications, which are mostly based on works by the author and his colleagues.

Recently, active spectral imaging attracts much attention as promising technology [3-8]. The active spectral imaging method has the possibility of recovering spectral reflectance information and estimating tristimulus values of object surface in high speed. We will introduce a spectral imaging technology by synchronizing a programmable light source and a high-speed monochrome

camera. The light source is capable of emitting arbitrary spectrum in high speed, so that the system has the advantage of capturing spectral images without using filters. First, a projector for spectrally rendering a real scene is described as a fundamental usage of the spectral imaging system. Second, the effective applications to spectral reflectance recovery and tristimulus imager are described.

Conventional Spectral Imaging Approach

Various imaging systems

Some representative spectral imaging systems incorporating typical filtration mechanisms are shown as follows:

(1) using one or two additional color filters to a trichromatic digital camera [9 , 10],

(2) combining a monochrome camera and color filters with different spectral bands [2],

(3) using narrow band interference filters [11 , 12], and

(4) using a liquid-crystal tunable (LCT) filter to a monochromatic camera [13 - 15].

Figure 2(a) shows a system of (1) for multi-band omnidirectional imaging which was realized with a trichromatic digital camera, a fisheye lens, color filters, and a rotating table. Figure 2(b) shows the spectral sensitivity functions of the camera. For multi-spectral image acquisition, we selected additional color filters and placed these between the lens and the camera body. Figure 2(c) shows the spectral transmittances of these filters. The filter SP-6 is effective for shifting the spectral sensitivities to the short wavelength and long wavelength, while SP-7 is effective for shifting the spectral sensitivities to the middle wavelength. An imaging system with six spectral bands in the visible wavelength region is produced by combining these transmittances to the original spectral sensitivities. Figure 2(d) shows the overall spectral-sensitivity functions of the present multi-spectral imaging system.

Figure 3(a) shows an imaging system of (3) consisting of a monochrome CCD camera, a C mount lens, an automatic filter changer, and eight interference filters. Figure 3(b) shows the composite spectral sensitivity functions for eight sensors. The interference filter utilizes the interference effect of light occurred by a dielectric material and a metal thin film. The spectral transmission characteristics of the interference filter depend on the index of refraction and the incidence angle. So we note that the registration error occurs in the acquired images by this type of imaging system.

Figure 4(a) shows an imaging system of (4) consisting of the LCT filter and a monochrome CCD camera using Peltier cooling to reduce noise. This filter provides a convenient type of filtering mechanism since spectral channels are narrow and variable by a computer control. Although narrow-band filtration is required from the standpoint of precise measurement of spiky spectra, the images by narrow bands are often dark and noisy. So the cooling system is needed to improve the SN ratio. The present band widths are about 10 nm in the visible range. Figure 4(b) represent the overall spectral-sensitivity functions in 61 channels.

Some of the shortcomings of the conventional systems are (1) latency time due to multiple capturing, (2) time consumption due to filter change, (3) difficulty in designing optimum filters, (4) accuracy inferior to a spectrometer, and (5) long exposure time because of low filter transmittances. Recently, a new type of sensor, called Transverse Field Detector (TFD) was proposed [16]. The sensitivities of this type of sensor are spectrally tunable by

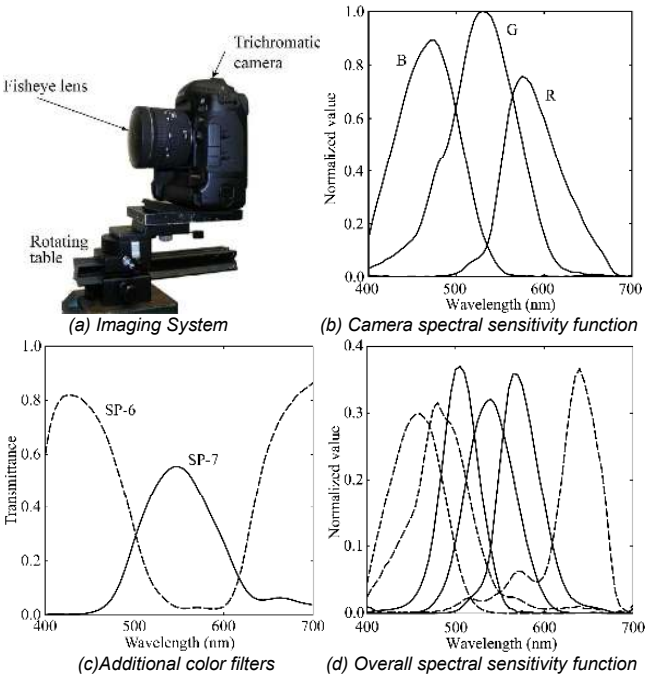

(a) Imaging System (b) Camera spectral sensitivity function

(c)Additional color filters (d) Overall spectral sensitivity function

***Figure 2**. Omnidirectional imaging system.*

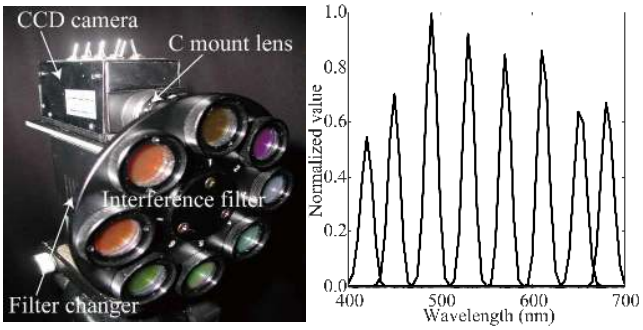

(a) Imaging System (b) Spectral sensitivity function

***Figure 3**. Imaging system using interference filters.*

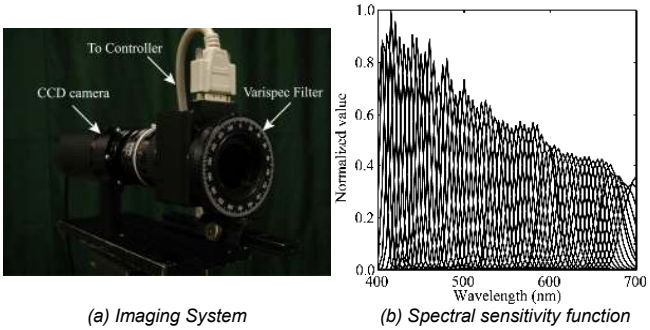

(a) Imaging System (b) Spectral sensitivity function

***Figure 4**. Imaging system using LCT filter.*

taking advantage of the light absorption of silicon. There are reported only preliminary simulations of a theoretical imaging system using the sensor [17]. It should be noted that these multi-spectral imaging systems are based on the filtration mechanism at the sensor side under passive illumination.

Estimation algorithms of spectral functions

First, we present algorithms for estimating color signals in a natural scene, which contains direct illuminations of daylights and indirect illuminations of the reflected lights from different object surfaces. Next, we present an algorithm for estimating spectral reflectance of an object surface under a known illuminant.

A. Color signals from low-dimensional camera data

If the imaging system is noise free, the sensor outputs are modeled as a linear system

$$\rho_i = \int_{400}^{700} E(\lambda)R_i(\lambda)d\lambda \ , \quad \text{(i=1, 2, ..., n)} \tag{1}$$

where n represents the number of sensors, $E(\lambda)$ is the color signal, $R_i(\lambda)$ is the spectral sensitivity function of the i-th sensor. If n is small, a finite-dimensional linear model is available for describing the continuous spectral functions by only a small number of basis functions. Let us express $E(\lambda)$ as a linear combination of m basis functions as

$$E(\lambda) = \sum_{i=1}^{m} \varepsilon_i E_i(\lambda) \quad , \tag{2}$$

where $\{ E_i(\lambda), i=1, 2, ..., m\}$ is a statistically determined set of basis functions, and $\{ \varepsilon_i \}$ is a set of weighting coefficients.

To derive the basis functions we created two spectral datasets for surface-spectral reflectances and light sources [18]. Concerning surface reflectance, we collected many objects from the real world. Figure 5(a) shows the set of spectral reflectance curves of 871 object surfaces. Concerning light source, we used the CIE standard illuminants with different correlated color temperatures from 5000K to 10000K and a small number of the direct measurements of the sky. Figure 5(b) shows the spectral distributions of nine light sources.

Next, a large database of about 8000 color signals was produced by multiplying the surface-spectral reflectances and the light source spectra. PCA was then applied to the database of color signals, and the basis functions were obtained as the first *m* principal components.

The illuminant weight vector $\boldsymbol{\varepsilon} = [\varepsilon_1, \varepsilon_2, ..., \varepsilon_m]^t$ is estimated from the sensor outputs in the form $\boldsymbol{\varepsilon} = \boldsymbol{\Lambda}^+\boldsymbol{\rho}(x)$ where $\boldsymbol{\rho}(x)$ is the sensor output vector and $\boldsymbol{\Lambda}^+$ is the generalized inverse of a *n* x *m* matrix $\boldsymbol{\Lambda}$ with (i, j) elements as $\left[\int E_j(\lambda)R_i(\lambda)d\lambda\right]$. In our experiments, *m* = 5 was the most appropriate.

B. Color signals from high-dimensional camera data

If the imaging systems have many sensor outputs in equal intervals, which are narrow band spectral sensitivities as shown in Figure 4(b), a direct method is adopted for effective estimation of natural scene color signals. Suppose that the visible range is segmented into a sequence of narrow wavelength bands with even intervals {red, yellow-red, yellow, green-yellow, ..}. A one-to-one mapping holds between the sensor output and the wavelength band.

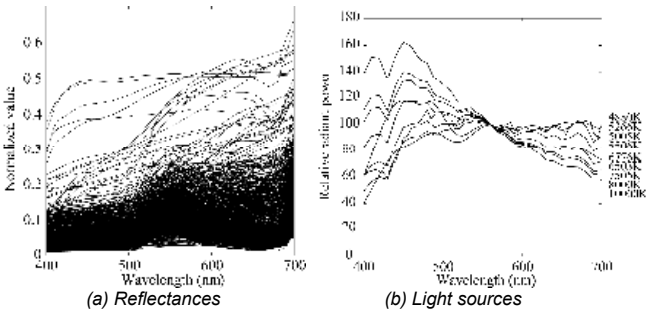

(a) Reflectances (b) Light sources

Figure 5*. Databases of surface-spectral reflectances for a variety of objects on university campus and spectral-power distribution for nine light sources.*

Let $\lambda_1, \lambda_2, ..., \lambda_n$ be the center wavelengths of the sensor spectral sensitivities. The narrow band condition of each sensor permits us to describe the sensor output as

$$\rho_i = E(\lambda_i)\int_{400}^{700} R_i(\lambda)d\lambda \ , \quad (i=1, 2, ..., n) \tag{3}$$

Therefore the spectral distribution of the color signal is estimated as a sequence of *n* numerical values.

$$E(\lambda_i) = \rho_i \Big/ \int_{400}^{700} R_i(\lambda)d\lambda \ . \quad (i=1, 2, ..., n) \tag{4}$$

C. Color signals from noisy camera data

The observed images can include various noise on sensors and optical process. Then the sensor outputs are described as

$$\rho_i = \int_{400}^{700} E(\lambda)R_i(\lambda)d\lambda + n_i, \quad (i=1, 2, ..., n) \tag{5}$$

where n_i is the noise component with zero mean. We sample each spectral function at *N* points with an equal interval $\Delta\lambda$ in [400, 700nm]. Let **e** be an *N*-dimensional column vector representing the color signal $E(\lambda)$ and **R** be an $n \times N$ matrix with the element $r_{ij} = R_i(\lambda_j)\Delta\lambda$, and define $\boldsymbol{\rho}$ be an *n*-dimensional column vector representing the sensor outputs. Then the above relationships are summarized in a linear matrix equation

$$\boldsymbol{\rho} = \mathbf{R}\,\mathbf{e} + \mathbf{n} \, . \tag{6}$$

When the signal **e** and the noise **n** are uncorrelated, the Wiener estimate $\hat{\mathbf{e}}$ is given as

$$\hat{\mathbf{e}} = \mathbf{C}_{ss}\mathbf{R}^t(\mathbf{R}\mathbf{C}_{ss}\mathbf{R}^t + \boldsymbol{\Sigma})^{-1}\boldsymbol{\rho} \ , \tag{7}$$

where $\mathbf{C}_{ss}$ is the correlation matrix of color signals $\mathbf{C}_{ss} = \mathbf{E}[\mathbf{e}\mathbf{e}^t]$ and $\boldsymbol{\Sigma}$ is the covariance matrix of noises $\boldsymbol{\Sigma} = \mathbf{E}[\mathbf{n}\mathbf{n}^t]$ (see [18]). We can assume that the noises in each spectral channel are statistically independent. In this case, the covariance matrix is reduced to be diagonal as $\boldsymbol{\Sigma} = \text{diag}(\sigma_1^2, \sigma_2^2, ..., \sigma_n^2)$.

The noise component includes image sensor noises based on thermal noise and shot noise, and an approximation error in the model. Estimation of the noise properties is not easy. Although there are several suggestions for this, we determined the SNR in an empirical way. The Wiener estimator relies upon the statistics of a data set to achieve the estimation. To determine the correlation matrix $\mathbf{C}_{ss}$ properly, we need a large database of color signals. For this purpose we can use the database, consisting of two spectral

datasets for surface-spectral reflectances and light sources shown in Figure 5.

D. Spectral reflectance from noisy camera data under a known illuminant

We consider recovering the surface spectral reflectance from the noisy sensor outputs, which are modeled as a linear system

$$\rho_i = \int_{400}^{700} S(\lambda)E(\lambda)R_i(\lambda)d\lambda + n_i, \quad (i=1, 2, ..., n) \qquad (8)$$

where $S(\lambda)$ is the spectral reflectance of an object surface, and $E(\lambda)$ is the illuminant spectrum. Let **s** be an N-dimensional column vector representing $S(\lambda)$, and **R** be an N x n matrix with the element $r_{ij} = E(\lambda_j)R_i(\lambda_j)\Delta\lambda$. The sensor output vector **ρ** is represented as $\boldsymbol{\rho} = \mathbf{R}\mathbf{s} + \mathbf{n}$. Note that this equation is the same fashion as (6). Therefore, if the illuminant $E(\lambda)$ is known in advance or measured directly using a spectro-radiometer and a standard white reference, the estimate of **s** can be given by the Wiener estimator [19].

Figure 6 demonstrates a small oil painting called "Flowers" used in our experiments and the estimation result of surface spectral reflectance in Area 3. The estimated spectra are depicted in bold curves, which are compared with the broken curves of the spectro-radiometer measurements and the dashed curves of the estimates by the RGB camera method. The multispectral imaging method recovers the spectral reflectances more precisely than the RGB system does.

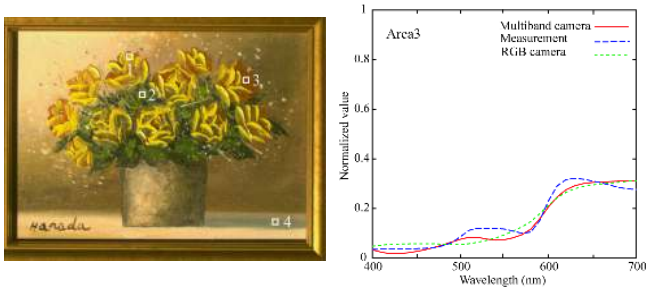

***Figure 6**. Estimation result of spectral reflectance in Area 3 of Oil painting "Flowers."*

Spectral Imaging Approach Using Active Illuminant

Imaging system

Figure 7 shows the spectral imaging system [20], consisting of a high speed monochrome camera (Epix SV643M), a programmable light source (Optronic Laboratories OL490), and a personal computer (PC) for controlling the camera and the light source. The light source uses digital micromirror device (DMD) is well used for realizing a spectrally controllable light. Figure 8 depicts the principle of the programmable light source using DMD technology. It is composed of a xenon lamp source, a grating, a DMD chip, and a liquid light guide. In this system, a light beam of xenon is separated by the grating into its constituent wavelengths. The wavelength and intensity information is controlled using the two-dimensional DMD chip, where one axis corresponds to the wavelength distribution of the spectrum, and the other axis to the intensity distribution. An advantage of the DMD-based programmable light source is that it can switch the output light spectrum much faster than a light source based on a liquid-crystal display [21 , 22].

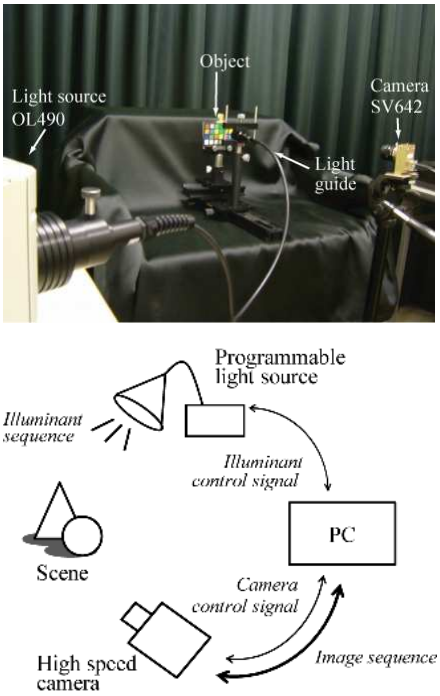

***Figure 7**. Spectral Imaging System*

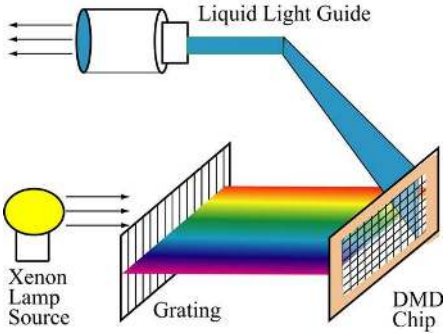

***Figure 8**. Principle of the programmable light source.*

Illuminant Control

The light source system can produce emissions at a single wavelength and broad spectrum. We design the emission of a spectral function in two modes of time sequence: steady-state and time-varying. In the steady-state mode, the same spectrum is generated at every time. While in the time-varying mode, different spectra can be generated at every time. Let $E_{\lambda i}(\lambda)$ be a spectral-power distribution emitted at a central wavelength λ_i and ($E_{\lambda 1}(\lambda)$, $E_{\lambda 2}(\lambda)$, …, $E_{\lambda n}(\lambda)$) be the time sequence. Figure 9 illustrates an example of spectral-power distributions generated as

a time sequence. A set of single spectral functions with narrow width of wavelength is generated at an equal wavelength interval in the visible range. Figure 9(a) is a 3D perspective view in the time-varying mode, where different spectral functions are depicted in the time series $E_{\lambda 1}(\lambda, t_1)$, $E_{\lambda 2}(\lambda, t_2)$, …, $E_{\lambda n}(\lambda, t_n)$. Figure 9(b) is the view in the steady-state mode, where the same spectrum is depicted as $E_{\lambda 1}(\lambda, t) + E_{\lambda 2}(\lambda, t) + ... + E_{\lambda n}(\lambda, t)$ at each time.

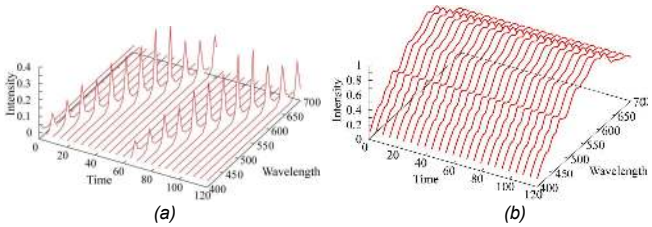

(a) (b)

***Figure 9**. Spectral-power distributions generated as a time sequence. (a) Time-varying mode, (b) Steady-state mode.*

Illuminant projection for spectral rendering

The feasibility of illuminant-spectral shape was extremely limited in the conventional lighting systems because the illuminant spectra were produced by combining several basis light sources of wide spectral bands. In contrast, the proposed imaging system enables us to observe object surfaces under illuminant with arbitrary spectral-power distribution. We examined the accuracy of illuminant spectra produced by the present system.

Human visual assessment of object surface appearance is often performed under typical light sources such as Illuminants A and D65. Figure 10 shows the illuminant spectral distributions for CIE Standard Illuminants A and D65, which were produced by our control system. The produced spectra are almost coincident with the target spectra.

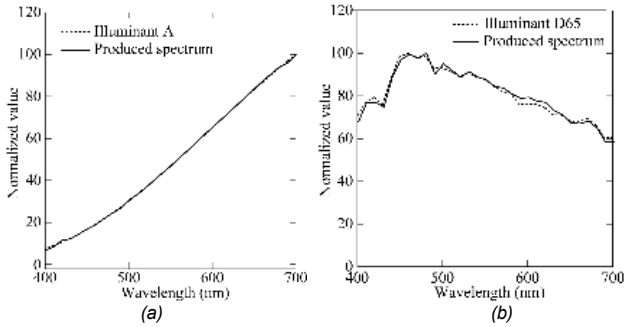

(a) (b)

***Figure 10**. Illuminant spectral distributions produced for CIE Standard Illuminants A and D65. (a) Illuminant A, (b) Illuminant D65.*

A visual assessment system for spectrally rendering 3D object surfaces in a real scene is constructed by producing illuminant with arbitrary spectral-power distribution in the present system. Figure 11 demonstrates the appearances of a flower decoration by projecting two different LED illuminants of about 6500K color temperature. Note that Figure 11 has real scene photographs captured by a digital camera. We confirmed that the color appearances of these photographs displayed on a calibrated sRGB monitor were close to the visual appearance. Figures 11(a) and (b) show the illuminant spectral power-distributions of a white LED and a RGB mixing LED, respectively. These illuminants were projected on the same object. The color temperatures of the illuminants are quite close with each other as (a) 6430K and (b) 6485K, and also the xy chromaticity coordinates are almost the same as (a) (x, y) = (0.313, 0.332) and (b) (x, y) = (0.314, 0.332). However, it is interesting to observe that the appearances of the colorful flower decoration are greatly distinguished under the two illuminants in Figures 11(c) and (d). Note that the former emphasizes the appearance of green colored surfaces, and the latter emphasizes the appearance of red colored surfaces. Thus, the color appearance is strongly affected by the illuminant spectral curve. Therefore, this projection system is useful for various purposes such as high-speed spectral rendering of a real scene, metamer detection, visual evaluation of surface appearance, and investigation of the Color Rendering Index.

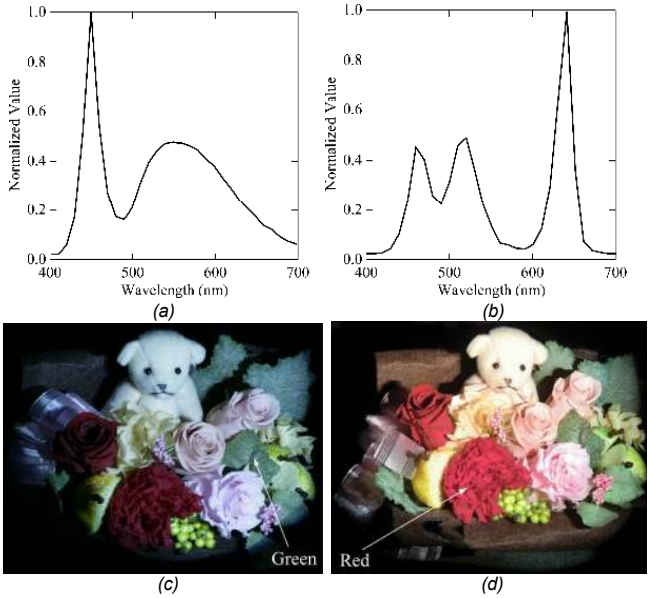

(a) (b) (c) (d)

***Figure 11**. Appearances of a flower decoration under different LED illuminants with 6500K color temperature. (a) SPD of White LED, (b) SPD of LED by mixing RGB, (c) Appearance of the flower decoration under illuminant (a), (d) Appearance of the flower decoration under illuminant (b).*

Applications

A. Spectral reflectance recovery

Surface-spectral reflectance can be recovered under active illumination. However, it was difficult to accomplish the active imaging system with merits in both computation time and recovering accuracy, because the previous methods employed broad band light sources, which consist of linear combination of the fixed spectral-power distributions of primary colors.

We solve the problem of spectral reflectance recovery effectively by using the present spectral imaging system. When the reciprocal function of the camera sensitivity is projected onto an

object surface as a time sequence of spectrum, the spectral reflectance is obtained directly from the camera outputs at the spatial resolution of camera pixels.

Let $S(\lambda)$ and $V(\lambda)$ be the surface-spectral reflectance function and the sensor-spectral sensitivity function, respectively. When an object surface is illuminated by a light source with spectrum $I(\lambda,t)$, the camera output at time t_i is described as

$$O(t_i)=\int S(\lambda)I(\lambda,t_i)V(\lambda)d\lambda . \quad (9)$$

If the spectral reflectance is smooth and the light source is a narrow-band illuminant $E_\lambda(\lambda,t)$ at the center wavelength λ, the camera output is rewrote as

$$O(t_i)=\int S(\lambda)E_{\lambda i}(\lambda,t_i)V(\lambda)d\lambda=S(\lambda_i)\left(\int E_{\lambda i}(\lambda,t_i)V(\lambda)d\lambda\right). \quad (10)$$

Here note that the sensor-spectral sensitivity function $V(\lambda)$ does not have to be sharp or rather should be broad enough in the visible wavelength range, because the illuminant is narrow in the present system. Since the bracketed term of Eq.(10) is independent of an object surface, we can calculate it in advance as $c_i=\int E_{\lambda i}(\lambda,t_i)V(\lambda)d\lambda$. When the surface is illuminated sequentially by the narrow-band spectrum with a moving center wavelength as shown in Figure 9(a), the surface-spectral reflectance ($S(\lambda_1), S(\lambda_2)$, …, $S(\lambda_n)$) can be estimated from the time sequence of the camera outputs ($O(t_1), O(t_2)$, …, $O(t_n)$) as $S(\lambda_i)=O(t_i)/c_i$.

If the basis illuminant $E_{\lambda i}(\lambda,t_i)$ is designed as a reciprocal function of $V(\lambda)$, the spectral reflectance is obtained directly from the camera output sequence ($O(t_1), O(t_2)$, …, $O(t_n)$), without computation.

The above recovering process consists of the sequential projection of *n* times. If spectral reflectance is represented by 61 wavelength points sampled with an equal interval of 5 nm in the range [400, 700nm], it needs 61 illuminant projections.

The linear finite-dimensional model of spectral reflectances is useful for accelerating the recovering process by reducing the number of illuminant projections. We suppose that the spectral reflectance function $S(\lambda)$ can be expressed as $S(\lambda)=\sum_{i=1}^{m}\sigma_i S_i(\lambda)$, where $\{S_i(\lambda),\ i=1,2,...,m\}$ is a statistically determined set of orthogonal basis functions for reflectances, and $\{\sigma_i,\ i=1,2,...,m\}$ is a set of scalar weights. In this case, we design the illuminant spectra as $I(\lambda,t)=S_i(\lambda)/V(\lambda)$, and the corresponding camera output as $O(t_i)=\sigma_i$. Then, the surface-spectral reflectance is recovered from the camera output sequence in the following form $S(\lambda)=\sum_{i=1}^{m}O(t_i)S_i(\lambda)$.

Obviously the basis functions take negative values except for the first basis, which are not optically realizable. The simplest way to solve this problem is to shift the functions upward by adding a constant bias as $S_i(\lambda)=S_i(\lambda)+K$ to take all positive values. In this case, we need an additional illuminant projection $I(\lambda,t_K)=K/V(\lambda)$ and an additional camera output $O(t_K)$. Other compensation algorithms is Epstein approximation [23], optimal non-negative filter [24], and non-negative matrix factorization [25 , 26] were also proposed for non-negative components.

In the present approach, a simple and effective way is recommended to separate the basis functions into both positive and negative parts, and make symmetric functions with respect to the zero-axis. The basis functions are described as $S_i(\lambda)=S_i^+(\lambda)-S_i^-(\lambda)$. Figure 12 depicts the illuminant spectra $\{S_i^+(\lambda)/V(\lambda)\}$ and $\{S_i^-(\lambda)/V(\lambda)\}$ as a set of the modified basis functions with all positive values, where the solid curves and the broken ones indicate the positive functions to $S_i^+(\lambda)$ and the symmetric functions to $S_i^-(\lambda)$, respectively. In this case, we need two projections corresponding to the positive and negative functions for each basis function except for the first basis. Then a pair of the camera outputs $O(t_{i+})$ and $O(t_{i-})$ is used for recovering spectral reflectance from the linear model equation with $\sigma_i=O(t_{i+})-O(t_{i-})$. When we adopt the five-dimensional linear model, the reflectance recovering process consists of nine illuminant projections. The number of projections is still much smaller than the one in the original sequential projection algorithm.

We examined the performances in reflectance estimation results using an X-Rite Mini Color Checker by the three algorithms. We use RMSE and the CIELAB color difference as metrics for spectral matching. The average RMSE and the average color differences ΔE_{ab}^* for all 24 color patches were 0.0153 and 2.52 under D65, respectively, when using the above symmetric basis functions. The frame rate for successively recovering the spectral reflectance images is about 13 fps in the present system.

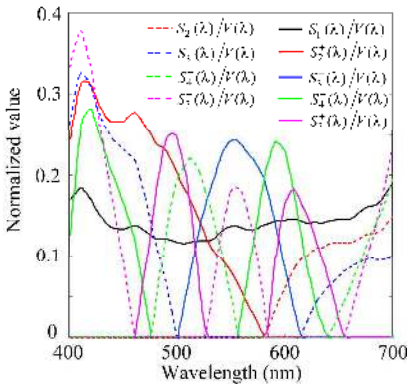

***Figure 12**. Illuminant spectra for the basis functions with positive values.*

B. Tristimulus Imager

Colorimetry is the scientific technology used to qualify and describe the human color perception physically. The CIE-XYZ tristimulus values are most often used as colorimetric values in representing the physical correlates of color perception. The traditional methods based on colorimeter or spectrometer cannot determine the tristimulus values at the pixel level of a color image, but determine the values for a broad area on the object surface at a time. It takes much time to obtain the precise color values. The present spectral imaging system using an active illuminant can be applied to a new type of technology aiming at high-speed and high-spatial resolution colorimetry. The new technology of the tristimulus imager is based on the projection of the modified color-

matching functions as illuminant. The CIE-XYZ values can then be obtained at the spatial resolution of camera pixels on the illuminated surface directly from the camera responses.

The tristimulus values X, Y, and Z of an object surface are calculated as

$$\begin{bmatrix} X \\ Y \\ Z \end{bmatrix} = \int S(\lambda) E_T(\lambda) \begin{bmatrix} \bar{x}(\lambda) \\ \bar{y}(\lambda) \\ \bar{z}(\lambda) \end{bmatrix} d\lambda , \tag{11}$$

where $E_T(\lambda)$ is a target illuminant, and $(\bar{x}(\lambda), \bar{y}(\lambda), \bar{z}(\lambda))$ are the CIE color-matching functions. In the traditional technology of colorimetry, the above calculation is performed using the light reflected from the object surface. In our new technology, if the target illuminant $E_T(\lambda)$, in which the object is observed, is specified like Illuminant D65 or Illuminant A, we can design the active illuminant to imitate the environment of observation.

Let $I(\lambda)$ be a linear combination of the basis spectra in the form $I(\lambda) = \sum_{i=1}^{n} c_i E_{\lambda i}(\lambda)$. Suppose that this set of basis spectra is projected to the object surface in the steady-state mode, the camera output is then described as

$$O = \int S(\lambda) I(\lambda) V(\lambda) d\lambda . \tag{12}$$

Therefore, the tristimulus values can be obtained by the camera outputs if three conditions are satisfied as

$$\begin{aligned} I_x(\lambda)V(\lambda) &= E_T(\lambda)\bar{x}(\lambda), \\ I_y(\lambda)V(\lambda) &= E_T(\lambda)\bar{y}(\lambda), \\ I_z(\lambda)V(\lambda) &= E_T(\lambda)\bar{z}(\lambda). \end{aligned} \tag{13}$$

Therefore, the problem is reduced to determining the weights c_1, c_2, …, c_n for the basis spectra at λ_1, λ_2, …, λ_n, so that the illuminant spectra are coincident with the modified matching functions $E_T(\lambda)\bar{x}(\lambda)/V(\lambda)$, $E_T(\lambda)\bar{y}(\lambda)/V(\lambda)$, and $E_T(\lambda)\bar{z}(\lambda)/V(\lambda)$. Since we use a monochrome camera, the camera outputs only one tristimulus value at one time. Therefore, the tristimulus values are obtained by three camera outputs $(O(t_1), O(t_2), O(t_3))$ in time sequence, where

$$\begin{bmatrix} O(t_1) \\ O(t_2) \\ O(t_2) \end{bmatrix} = \int S(\lambda) \begin{bmatrix} I_x(\lambda, t_1) \\ I_y(\lambda, t_2) \\ I_z(\lambda, t_3) \end{bmatrix} V(\lambda) d\lambda . \tag{14}$$

The tristimulus values are obtained at every pixel point of the object surfaces in an image.

Figure 13 shows the illuminant spectra $(I_x(\lambda,t_1), I_y(\lambda,t_2), I_z(\lambda,t_3))$ that were produced in order to obtain the XYZ tristimulus values under the CIE Standard Illuminants D65 and A by the present system. The broken curves represent the target spectra, which are the weighted matching functions ($E_{\mathrm{D65}}(\lambda)\bar{x}(\lambda)/V(\lambda)$, $E_{\mathrm{D65}}(\lambda)\bar{y}(\lambda)/V(\lambda)$, $E_{\mathrm{D65}}(\lambda)\bar{z}(\lambda)/V(\lambda)$) in (a) and ($E_{\mathrm{A}}(\lambda)\bar{x}(\lambda)/V(\lambda)$, $E_{\mathrm{A}}(\lambda)\bar{y}(\lambda)/V(\lambda)$, $E_{\mathrm{A}}(\lambda)\bar{z}(\lambda)/V(\lambda)$) in (b), where $(E_{\mathrm{D65}}(\lambda), E_{\mathrm{A}}(\lambda))$ indicate the illuminant spectral power distributions, and $(\bar{x}(\lambda), \bar{y}(\lambda), \bar{z}(\lambda))$ indicate the CIE 1931 color-matching functions in this case. We performed an experiment of colorimetry, where the above illuminants were projected to the X-Rite Mini ColorChecker. The accuracy was evaluated by the CIELAB color difference. The average color differences of ΔE^*_{ab} for all 24 color patches were 2.43 and 2.82 under Illuminant D65 and Illuminant A, respectively. The weighted color-matching functions were sequentially projected from the liquid guide cable to the object at 200 fps and the camera captured the scene of the illuminated object synchronously.

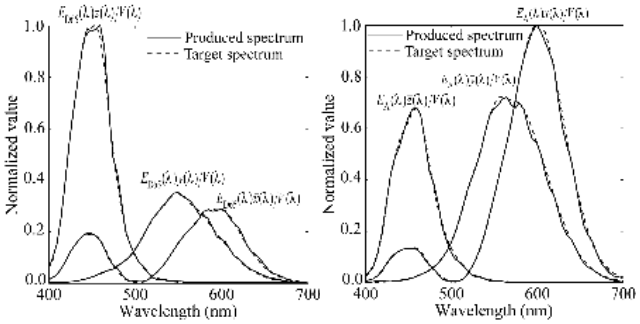

Figure 13*. Illuminant spectra produced for obtaining the tristimulus values under (a) Illuminant D65 and (b) Illuminant A.*

Conclusions

Multispectral imaging technology is a useful technology that is now widespread in all fields related with visual information. . We have discussed a variety of multi-spectral imaging methods for acquiring spectral information from a scene. First, conventional multispectral imaging approach was reviewed. The conventional imaging systems were mostly constructed by multi-band imaging devices with different filtration mechanism at the sensor side under passive illumination. We showed several imaging devices, estimation algorithms, and applications. Recently, active spectral imaging attracts attention as promising technology. We introduced an imaging system by synchronizing a programmable light source and a high-speed monochrome camera. Moreover, two effective applications to spectral reflectance recovery and tristimulus imager are described. Application in the field is expanding.

References

[1] P.D. Burns and R.S. Berns, "Analysis of multispectral image capture," Proc. 4th Color Imaging Conf. (CIC4), 19-22 (1996).

[2] S. Tominaga, "Multichannel vision system for estimating surface and illuminant functions," J. Opt. Soc. Am. A, **13(**11), 2163-2173 (1996).

[3] F. Xiao, J. M. DiCarlo, P. B. Catrysse, and B. A. Wandell, "Image analysis using modulated light sources," Proc. SPIE, **4306**, 22-30 (2001).

[4] J.-I. Park, M.-H. Lee, M. D. Grossberg, and S. K. Nayar, "Multispectral imaging using multiplexed illumination," Proc. 11th IEEE Inter. Conf. Comput .Vis. (ICCV), 1-8 (2007)

[5] J. M. DiCarlo, F. Xiao and B. A. Wandell, "Illuminating illumination," Proc. 9th Color Imaging Conf. (CIC9), 27-34 (2001).

[6] C. Chi, H. Yoo, M. Ben-Ezra, "Multi-spectral imaging by optimized wide band Illumination," Int. J. Computer Vision, **86**, 140–151 (2010)

[7] A. Mohan, R. Raskar, and J. Tumblin, "Agile Spectrum Imaging: Programmable Wavelength Modulation for Cameras and Projectors," Computer Graphics Forum,.**27**, 709-717 (2008).

[8] S. Tominaga and T. Horiuchi, "Spectral Imaging by Synchronizing Capture and Illumination," J. Opt. Soc. Am. A, **29** (2012)(to appear)..

[9] F. H. Imai and R. S. Berns, "Spectral estimation using trichromatic digital camera," Proc. the International Symp. Multispectral Imaging and Color Reproduction for Digital Archives, 42–49 (1999).
[10] S. Tominaga, T. Fukuda, and A. Kimachi, "A high-resolution imaging system for omnidirectional illuminant estimation," J. Imag. Sci. and Tech., **52**, 040907-1 (2008).
[11] S. Nishi and S. Tominaga, "Calibration of a multispectral camera system using interference filters and its application," Proc. the Congress of the International Colour Association (2009).
[12] N. Shimano, K. Terai and M. Hironaga, "Recovery of spectral reflectances of objects being imaged by multispectral cameras," J. Opt. Soc. Am. A, **24**, 3211-3219 (2007).
[13] S. Tominaga, "Spectral imaging by a multi-channel camera," J. Elect. Imag., **8**, 332-341 (1999).
[14] M. A. López-Álvarez, J. Hernández-Andrés and J. Romero, "Developing an optimum computer-designed multispectral system comprising a monochrome CCD camera and a liquid-crystal tunable filter," Applied Optics, **47**, 4381-4390 (2008).
[15] M. A. López-Álvarez, J. Hernández-Andrés, J. Romero, J. Campos and A. Pons, "Calibrating the elements of a multispectral imaging system," J. Imag. Sci. and Tech., **53**, 031102-031102-10 (2009).
[16] G. Langfelder, A. F. Longoni and F. Zaraga, "Implementation of a multi-spectral color imaging device without color filter array," Proc. SPIE, **7876**, 787606-1-787606-9 (2011).
[17] A. L. Lin, and F. Imai, "Efficient spectral imaging based on imaging systems with scene adaptation using tunable color pixels," Proc. 19th Color Imaging Conf. (CIC19), 332-338 (2011).
[18] S. Tominaga, A. Matsuura, and T. Horiuchi, "Spectral Analysis of Omnidirectional Illumination in a Natural Scene," J. Imag. Sci. and Tech., **51**(4), 040502-1 - 040502-9 (2010).
[19] S. Tominaga and N. Tanaka, "Spectral Image Acquisition, Analysis, and Rendering for Art Paintings," J. Elect. Imag., **17(**4), 043022.1-043022.13 (2008).
[20] S. Tominaga, T. Horiuchi, H. Kakinuma and A. Kimachi, "Spectral imaging with a programmable light source," Proc. 17th Color Imaging Conf. (CIC17), 133-138 (2009).
[21] M. Hauta-Kasari, K. Miyazawa, S. Toyooka and J. Parkkinen, "Spectral vision system for measuring color images," J. Opt. Soc. Am. A, **16**, 2352-2362 (1999).
[22] I. Farup, J. H. Wold, T. Seim, and T. Søndrol, "Generating light with a specified spectral power distribution," Applied Optics, **46**, 2411-2422 (2007).
[23] D.W. Epstein, "Colorimetric analysis of RCA color television system," RCA Rev., **14**, 227-258 (1953).
[24] G. Sharma, H. J. Trussell and M. J. Vrhel, "Optimal Nonnegative Color Scanning Filters," IEEE Trans. Image Process., **7**(1), 129-133 (1998).
[25] D. D. Lee and H. S. Seung, "Learning the parts of objects by non-negative matrix factorization," Nature, **401**, 788-791 (1999).
[26] G. Buchsbaum and O. Bloch, "Color categories revealed by non-negative matrix factorization of Munsell color spectra," Vis. Res., **42**, 559-563 (2002).

Author Biography

Shoji Tominaga received the B.E., M.S., and Ph.D. degrees in electrical engineering from Osaka University, Japan, in 1970, 1972, and 1975, respectively. From 1976 to 2006, he had been with Osaka Electro-Communication University. Since 2006, he is a professor at Graduate School of Advanced Integration Science, Chiba University. During the 1987-1988 academic years he was a Visiting Scholar at the Department of Psychology, Stanford University. He is a fellow of IEEE, IS&T, SPIE and IEICEJ.